Earth and Planetary Science Letters 530 (2020) 115890

Contents lists available at ScienceDirect

Earth and Planetary Science Letters

www.elsevier.com/locate/epsl

The impact of Early Cretaceous gateway evolution on ocean circulation and organic carbon burial in the emerging South Atlantic and Southern Ocean basins

W. Dummann [a,c,*], S. Steinig [b], P. Hofmann [a], S. Flögel [b], A.H. Osborne [b], M. Frank [b], J.O. Herrle [c,d], L. Bretschneider [b], R.M. Sheward [c], T. Wagner [e]

[a] Institute of Geology and Mineralogy, University of Cologne, Zülpicher Str. 49a, D-50674 Cologne, Germany
[b] GEOMAR Helmholtz Centre for Ocean Research Kiel, Wischhofstr. 1-3, D-24148 Kiel, Germany
[c] Institute of Geosciences, Goethe-University Frankfurt, Altenhöferallee 1, D-60438 Frankfurt am Main, Germany
[d] Biodiversity and Climate Research Centre (BIK-F), Senckenberganlage 25, D-60325 Frankfurt am Main, Germany
[e] Lyell Centre, School of Energy, Geoscience, Infrastructure and Society, Heriot-Watt University, Edinburgh, EH14 4AS, UK

ARTICLE INFO

Article history:
Received 12 July 2019
Received in revised form 6 September 2019
Accepted 8 October 2019
Available online 24 October 2019
Editor: L. Robinson

Keywords:
Early Cretaceous
South Atlantic
ocean circulation
neodymium isotopes
gateways
organic carbon burial

ABSTRACT

Organic carbon burial is an important driver of carbon cycle and climate dynamics on geological and shorter time scales. Ocean basins emerging during the Early Cretaceous break-up of Gondwana were primary sites of organic carbon burial, implying that their tectonic and oceanographic evolution may have affected trends and perturbations in global climate via changes in local organic carbon burial. Assessing the role of individual ocean basins in the global carbon-climate context requires a sound understanding of the processes that induced large-scale changes in carbon burial and the timing of these changes. Here we reconstruct the oceanographic evolution, and its links to organic carbon burial, in the Barremian to Albian South Atlantic and Southern Ocean basins, which may have acted as carbon sinks of global importance. Our reconstruction is based on combined seawater neodymium isotope and sedimentological records obtained from multiple deep sea drill sites and a new general circulation model. Deep water circulation within and between those basins was primarily controlled by the opening of the shallow Falkland Plateau Gateway (between ∼118 Ma and ∼113 Ma) and the deep Georgia Basin Gateway (by ∼110 Ma), for which we provide new age constraints based on biostratigraphic and carbon isotope data. The opening of these gateways was accompanied by local to basin-wide decreases in organic carbon burial, suggesting that ocean circulation affected the oxygenation state via changes in deep water ventilation. Although our data do not provide quantitative information on the impact of changes in regional organic carbon burial on the global carbon cycle, the synchronicity between the reduction of organic carbon burial in the South Atlantic basin and global warming during the Early Albian points to a strong causal relationship.
Crown Copyright © 2019 Published by Elsevier B.V. All rights reserved.

1. Introduction

Long-term (10^6 to 10^7 yr) variations of atmospheric CO_2 concentration are controlled by a variety of processes including degassing from volcanism and metamorphism, and drawdown by silicate weathering and sedimentary burial of organic carbon (OC) (Berner, 1990). On such geological time scales, the temporal and spatial distribution of marine OC burial has been closely related to the tectonic development of ocean basins, which form major depocenters of OC during their early evolutionary stages (Trabucho Alexandre et al., 2012). This turns emerging ocean basins into large-scale carbon sinks, the development and disappearance of which affects global climate trends (McAnena et al., 2013).

The opening of the South Atlantic and Southern Ocean during the break-up of Gondwana in the Early Cretaceous (Pérez-Díaz and Eagles, 2017) provides an ideal case study to investigate the multi-scale relationships between tectonics, ocean circulation, biogeochemistry, and climate. Sedimentological evidence including extensive Aptian black shale deposits recovered at several deep sea drill sites (Arthur and Natland, 1979; Zimmerman et al., 1987) and prolific hydrocarbon reservoirs along continental margins (Katz and Mello, 2000) indicate that prolonged episodes of intense marine OC burial must have occurred in the emerging South Atlantic basins. Recent biogeochemical modeling suggests that OC burial in the South Atlantic may have contributed substantially to global carbon cycle and climate dynamics during the

* Corresponding author at: Institute of Geology and Mineralogy, University of Cologne, Zülpicher Str. 49a, D-50674 Cologne, Germany.
E-mail address: wdummann@uni-koeln.de (W. Dummann).

https://doi.org/10.1016/j.epsl.2019.115890
0012-821X/Crown Copyright © 2019 Published by Elsevier B.V. All rights reserved.

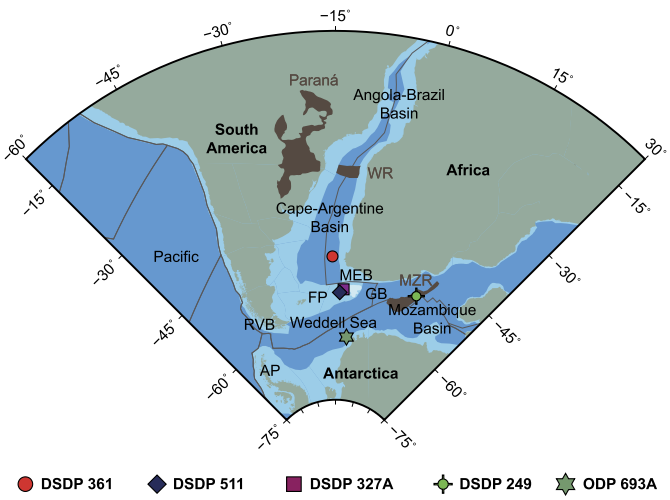

Fig. 1. Mid-Aptian (115 Ma) plate tectonic reconstruction of the South Atlantic and Southern Ocean (Matthews et al., 2016). Distribution of land masses (olive green) is based on the modern coastline. Brown shaded areas represent igneous provinces (Paraná large igneous province, Walvis Ridge (WR), and Mozambique Ridge (MZR)) discussed in the text. RVB: Rocas Verdes Basin, AP: Antarctic Peninsula, FP: Falkland Plateau, MEB: Maurice Ewing Bank (white shaded area), GB: Georgia Basin. (For interpretation of the colors in the figure(s), the reader is referred to the web version of this article.)

Aptian (McAnena et al., 2013). Previous studies hypothesized that the magnitude of OC burial was closely linked to the Aptian-Albian opening of the South Atlantic-Southern Ocean gateway, which had a main control on ocean circulation within and between both basins (Arthur and Natland, 1979; Zimmerman et al., 1987). The timing of these gateway openings and their exact control on ocean circulation, OC burial, and, ultimately, climate are the focus of this study.

Here we present an improved model for the evolution of Early Cretaceous gateway opening in the southern South Atlantic using new geochemical data complemented by a novel general circulation modeling approach. Our study is based on a consistent Barremian to Albian stratigraphic framework combining biostratigraphic information with new stable carbon isotope data for five Deep Sea Drilling Project (DSDP) and Ocean Drilling Project (ODP) drilling sites (Fig. 1). We trace changes in ocean circulation and water mass mixing based on radiogenic neodymium (Nd) isotope signatures of past deep water masses and their mixtures to identify key phases in the opening of two marine gateways located on the Falkland Plateau and in the Georgia Basin (Fig. 1). The seawater Nd isotope composition serves as a quasi-conservative tracer of bottom water masses in the open ocean (cf. Frank, 2002). Nearshore waters mainly obtain their Nd isotopic signature ($^{143}Nd/^{144}Nd$, expressed as $\varepsilon_{Nd}(t)$) by continental weathering inputs from the surrounding areas (Piepgras and Wasserburg, 1980). Differences in seawater $\varepsilon_{Nd}(t)$ signatures of water masses are preserved along their flow paths (Piepgras and Wasserburg, 1980) due to the residence time of Nd in seawater, which is similar to the global ocean mixing time (Tachikawa et al., 1999). Hence, changes in seawater $\varepsilon_{Nd}(t)$, reliably recorded by early diagenetic ferromanganese coatings of sediment particles (Blaser et al., 2016), reflect water mass provenance, water mass mixing and changes in continental weathering inputs to the source areas of the water masses. The interpretations of our new seawater Nd isotope records are supported by a fully coupled atmosphere-ocean-sea ice general circulation model (Kiel Climate Model; Park et al. (2009)), adapted to Aptian-Albian boundary conditions. We combine proxy and model data to show that ocean circulation controlled by the opening of the Falkland Plateau and Georgia Basin Gateways preconditioned the young South Atlantic basin for large-scale enhanced OC burial between at least 128 Ma and 113 Ma.

2. Materials and methods

2.1. Site selection

The data of this study were extracted from the sediments of five DSDP and ODP Sites located at different paleo-water depths, which represent the stratigraphically best constrained records currently available for the southern South Atlantic and Southern Ocean (Fig. 1). DSDP Site 361 was drilled in the Cape Basin on the lower continental rise of South Africa (Bolli et al., 1978) and the recovered sediments mainly consist of Lower Aptian black shales and intercalated turbidite-derived sandstones (Natland, 1978), which are overlain by Upper Aptian to Lower Albian gray shales and reddish nannofossil claystones. Sampling at this site was restricted to hemipelagic mudstones, whereby turbidite layers were carefully avoided. Paleo-water depth estimates based on back-stripping range between 2000 and 2500 m (Melguen, 1978 and references therein), which agrees well with recent reconstructions of the Aptian Cape Basin paleo-bathymetry (Pérez-Díaz and Eagles, 2017).

DSDP Site 511 and Hole 327A are located in the eastern part of the Falkland Plateau Basin (Barker et al., 1977; Ludwig et al., 1983). Similar lithological sequences were recovered at the two sites and comprise black shales of unspecified Neocomian to Aptian age and Aptian to Albian gray to reddish brown muddy nannofossil chalk. Assemblages of sparse benthic foraminifera obtained from the Aptian black shale sequence at Site 511 indicate an outer shelf environment (Basov and Krasheninnikov, 1983), which is consistent with Albian paleo-bathymetric reconstructions based on benthic foraminifera at Site 511 and Hole 327A indicating an outer shelf to middle bathyal environment with estimated paleo-water depths of ∼800 m and ∼600 m, respectively (Holbourn et al., 2001).

From the Southern Ocean, two sites were investigated. ODP Hole 693A was drilled on a mid-slope bench located close to the Antarctic coast in the Weddell Sea (Barker et al., 1988). The drilling terminated in Upper Aptian to Albian OC-rich claystones. Paleo-water depth estimates based on benthic foraminifera yielded an upper bathyal (200–500 m) depth (Leckie, 1990). DSDP Site 249 is located on the Mozambique Ridge. The dominant Early Cretaceous lithology is volcanic claystone. A recent revision of the initial biostratigraphy showed that the basal sediments at Site 249 are not older than Barremian and that the sequence investigated in this study most likely ranges from the Barremian to Lower Aptian (Dunay et al., 2018). Weissert (1981) ascribed a paleo-water depth of 200 m to Site 249.

2.2. Total organic carbon and stable carbon isotope analysis

Total carbon (TC) content, total organic carbon (TOC) content, and total inorganic carbon (TIC) content were measured using a DIMATOC 100 carbon analyzer (Dimatec Corp., Germany). TIC content was measured as CO_2 gas after treatment with phosphoric acid at 160 °C. TC content was determined by combustion of the bulk sediment at 900 °C. TOC content was calculated from the difference between TC and TIC contents.

Carbon isotope analyses were performed on bulk carbonate and bulk organic matter. For bulk organic matter analysis, an aliquot of the samples was repeatedly treated with 10% hydrochloric acid at 50 °C, neutralized by washing with deionized water, and subsequently dried. Carbon isotope analyses were performed at the Goethe-University Frankfurt using a Flash Elemental Analyzer 1112 (Thermoquest) coupled to an MAT 253 gas source mass spectrometer via a continuous flow inlet. The USGS 24 standard was analyzed

repeatedly along with the samples to monitor accuracy and precision. Standards reproduced within ±0.2‰. Carbon isotope ratios ($\delta^{13}C$) are reported relative to the Vienna-Pee Dee belemnite standard (VPDB).

2.3. Neodymium isotope analysis

Neodymium isotope analyses were performed at GEOMAR Kiel. Seawater Nd isotope compositions were leached from authigenic ferromanganese coatings of bulk sediment particles following established protocols (Blaser et al., 2016). Sediment samples were first rinsed with ultrapure water and then leached for 60 min using a solution of 0.005 M hydroxylamine hydrochloride, 0.001 M Na-EDTA, and 1.5% acetic acid, buffered at pH 4. An aliquot of the leachate was taken, dried and reacted with concentrated nitric acid to remove hydroxylamine hydrochloride. Rare earth elements were isolated from the leachate by cation exchange chromatography (0.8 mL AG50W-X12 resin, 200–400 µm mesh; Barrat et al. (1996)). Neodymium was further separated from the rare earth elements using Ln-spec resin (2 mL, 50–100 µm mesh; Le Fèvre and Pin (2005)). The purified Nd fraction was treated with concentrated H_2O_2 to decompose residual organic matter.

Detrital Nd isotope signatures were obtained from residues of the sediment leaching procedures after dissolution via alkaline fusion following published protocols (Bayon et al., 2009). Prior to alkaline fusion the sediment residues were leached with a solution of 0.05 M hydroxylamine hydrochloride, 0.01 M Na-EDTA, and 15% acetic acid for 24 h to ensure complete removal of the authigenic ferromanganese coatings. For the fusion, sediments were placed in a crucible and treated with 1.2 g Na_2O_2 and 0.6 g NaOH at 650 °C for 15 min. The melt was dissolved and iron hydroxides were precipitated with ultra-pure water, transferred into PTFE vials and heated to 130 °C for 2 h to achieve complete co-precipitation of the rare earth elements. The solution was centrifuged and the supernatant was decanted. The iron hydroxide residue was dissolved in 6 M HCl and the neodymium was then separated and purified using the same chromatographic procedure as for the leachate samples.

Neodymium isotope measurements were mainly performed on a Nu Instruments MC-ICP-MS and some samples were measured on a Neptune Plus MC-ICP-MS, which have been demonstrated to be fully compatible by repeated measurements of the same reference samples. The $^{143}Nd/^{144}Nd$ results were normalized to the accepted value of the JNdi-1 standard measured repeatedly during the sample runs at the same concentration as the samples ($^{143}Nd/^{144}Nd = 0.512115$; Tanaka et al. (2000)). The external reproducibility (2σ) was determined based on repeated measurements of a SPEX standard solution serving as a second internal standard and was between 0.15 and 0.47 ε_{Nd} units. Nd isotope ratios are reported as $\varepsilon_{Nd} = ([(^{143}Nd/^{144}Nd)_{sample}/(^{143}Nd/^{144}Nd)_{CHUR}] - 1) * 10000$ with $(^{143}Nd/^{144}Nd)_{CHUR} = 0.512638$ (Wasserburg et al., 1981). Measured Nd isotope signatures were corrected for the in-situ decay of ^{147}Sm ($\varepsilon_{Nd}(t)$) using an average ferromanganese crust value of $^{147}Sm/^{144}Nd = 0.115$ for leachates (Ling et al., 1997) and average upper crust $^{147}Sm/^{144}Nd = 0.109$ for detrital samples (Taylor and McLennan, 1985).

2.4. Nannofossil biostratigraphy

We investigated 99 samples from Site 361 (core 48 to 28) to revise the Early to Late Aptian calcareous nannofossil biostratigraphy of Proto Decima et al. (1978). Samples were prepared using standard smear slide techniques for organic-rich sediments. Freshly cut rock fragments were scratched to produce a rock-powder, which was diluted with a mixture of buffered deionized water (NH_3, pH 8.5) and Triton X to lower the surface tension. The suspension was homogenized in an ultrasonic bath for one minute. About four drops of the suspension were distributed on a glass slide with a wooden toothpick and mounted using a Norland Optical Adhesive 61. Each sample was studied for about 20 min in random traverses to detect the main nannofossil biostratigraphic maker species and diversity using a ZEISS AxioImager 2 photomicroscope at a magnification of ×1250. Taxa considered here are listed in Supplementary Table 1. Bibliographic references for these taxa are given in Perch-Nielsen (1985), Bown et al. (1998) and Microtax (http://www.mikrotax.org/Nannotax3/index.html).

2.5. Age control and carbon isotope stratigraphy

Cross-correlation of all investigated sedimentary sequences is primarily based on published biostratigraphy and our new calcareous nannofossil data at Site 361. Cross-correlation was further refined by stable carbon isotope stratigraphy using new bulk $\delta^{13}C_{carb}$ and $\delta^{13}C_{org}$ records, which were correlated to the reference curve compiled by Herrle et al. (2015). Correlation was carried out using characteristic carbon isotope segments (CIS), which were revised according to Bottini et al. (2015) and extended into the Barremian (B1 to B8) according to Wissler et al. (2003) (Fig. 2a). Age models were constructed based on linear interpolation between biostratigraphic datums and carbon isotope stratigraphic tie points. The age models are presented in Fig. 2. In addition to our preferred age models, we report potential age ranges of individual stratigraphic segments (i.e., stratigraphically continuous sections of records, which are separated from each other by stratigraphic discontinuities), to account for age uncertainties related to the low stratigraphic coverage of some studied sediment sequences. A more detailed discussion on the stratigraphy of the study sites and the tie points used to construct the age models are provided in the supplementary material.

2.6. General circulation modeling

The modeling experiment was performed with the Kiel Climate Model (Park et al., 2009), a fully coupled atmosphere-ocean-sea ice general circulation model. The atmospheric component employs the ECHAM5 spectral model with a T42 horizontal resolution (∼2.8° × 2.8°) and 19 vertical levels (Roeckner et al., 2003). The ocean-sea ice component NEMO uses a 2° Mercator mesh and 31 unequally-spaced vertical levels (Madec, 2008). The meridional ocean resolution is increased to 0.5° in the equatorial region. Global topography and bathymetry are based on existing reconstructions of Müller et al. (2008) and Blakey (2008) and are described in detail in Blöhdorn (2013). Paleo-bathymetry of the study area was adapted from the Early Albian boundary conditions of Sewall et al. (2007) with an updated representation of the Falkland Plateau that rules out deep water mass exchange between the South Atlantic and the Southern Ocean (Pérez-Díaz and Eagles, 2017). River routing strictly follows the orography (Hagemann and Dümenil, 1997) and simplified zonal mean vegetation properties were applied. No permanent land ice was assumed to exist, although seasonal snowfall and sea ice formation is permitted in the model. Atmospheric CO_2 concentrations were set to 1200 ppmv, within the range (500 to 1300 ppmv) of most recent Aptian-Albian CO_2 reconstructions based on stomatal indices of fossil conifers (Jing and Bainian, 2018). The solar constant was reduced by ∼1% and set to 1350 W/m^2. The simulation was initialized with the output of an existing 6000 yr-long control integration with slightly different bathymetry. The experiment was integrated for an additional 3000 yr after which the change in the globally depth-integrated ocean temperature for the last 1000 model years was below 0.1 °C. Results are averaged over the last 500 yr of integration (Supplementary Fig. 4).

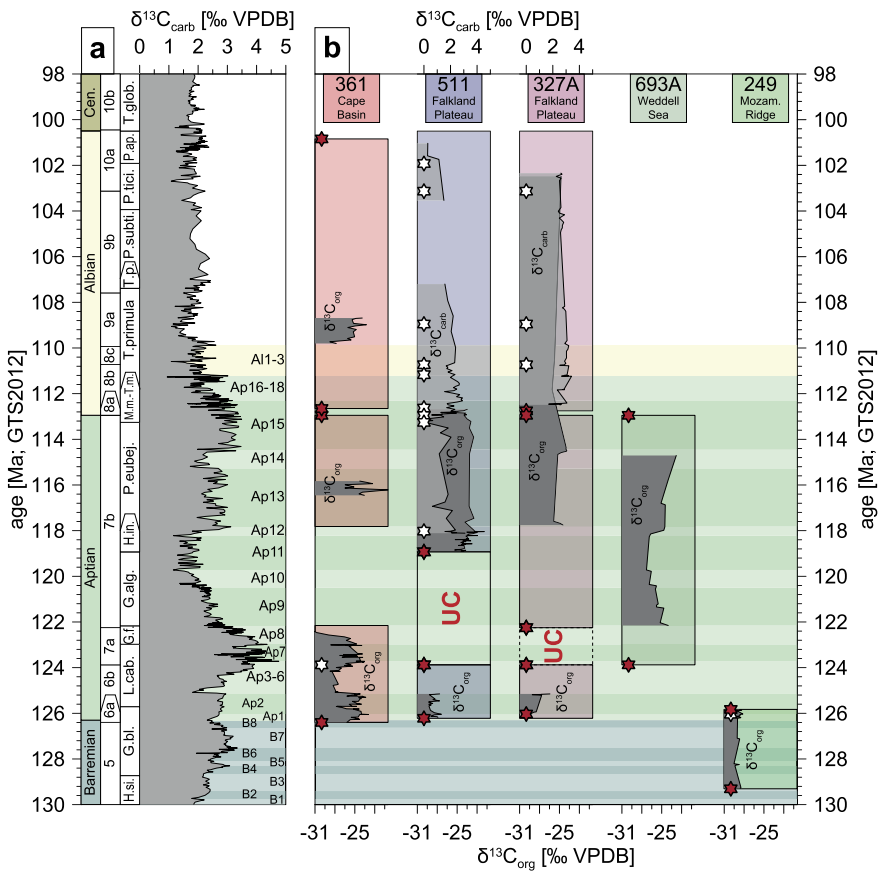

Fig. 2. (a) Low latitude carbon isotope record curve compiled by Herrle et al. (2015) plotted against the standard chronostratigraphy, calcareous nannofossil zonation (NC), and planktonic foraminiferal zonation (Gradstein et al., 2012). Barremian (B1 to B8) and Aptian to Albian (Ap1 to Al3) carbon isotope segments were assigned according to Wissler et al. (2003) and Bottini et al. (2015), respectively. (b) Carbon isotope records of DSDP Site 361, DSDP Site 511, DSDP Hole 327A, ODP Hole 693A, and DSDP Site 249 ($\delta^{13}C_{org}$: dark gray, $\delta^{13}C_{carb}$: light gray) plotted against age using our preferred age model for each site. Age uncertainties of different stratigraphic segments are indicated by color-filled boxes. Red stars represent biostratigraphic datums used to obtain minimal and maximal age constraints for stratigraphic segments. White stars indicate additional biostratigraphic tie points used to construct age models. UC: unconformity.

3. Results

3.1. Evolution of Nd-isotope signatures and organic carbon burial

The incomplete stratigraphic coverage at some study sites (i.e., due to spot coring, low recovery, and unconformities) and uncertainties in the age models prevent a continuous reconstruction of water mass evolution and OC accumulation. However, we are able to define three phases, which are clearly distinguishable within the limitations of stratigraphic resolution and age model accuracy (Fig. 3): (1) Late Barremian to Early Aptian (∼129 Ma to ∼124 Ma), (2) Late Aptian (∼118 Ma to ∼113 Ma), and (3) Middle to Late Albian (∼110 Ma to ∼100.5 Ma).

During phase 1 (∼129 Ma to ∼124 Ma), seawater $\varepsilon_{Nd}(t)$ signatures of −3.2 to −4.2 are recorded at Site 511 and Hole 327A, both located at upper bathyal water depths (600–800 m) on the Falkland Plateau. These seawater $\varepsilon_{Nd}(t)$ signatures are distinct from contemporaneous $\varepsilon_{Nd}(t)$ signatures of the detrital fraction, which yielded an $\varepsilon_{Nd}(t)$ value of −5.2. Site 249 located on the Mozambique Ridge (∼200 m paleo-water depth) recorded seawater $\varepsilon_{Nd}(t)$ signatures between −2.5 and −4.7, indistinguishable from the Falkland Plateau. Site 361 located at bathyal water depths (2000–2500 m) in the Cape Basin recorded markedly less radiogenic seawater $\varepsilon_{Nd}(t)$ signatures between −4.9 to −6.9, while the corresponding detrital $\varepsilon_{Nd}(t)$ values range between −8.1 and −3.7. During phase 1, black shales deposited at Site 361 contain 3% to 20% TOC and up to 8.6% TOC on the Falkland Plateau, whereas the gray shales of Site 249 only contain 1 to 2.5% TOC.

TOC and $\varepsilon_{Nd}(t)$ trends between phases 1 and 2 (∼124 Ma to ∼118 Ma) at Site 361 and on the Falkland Plateau are poorly constrained due to the low stratigraphic coverage and a ∼6 Ma long hiatus, respectively. At Hole 693A located in the Weddell Sea (200–500 m paleo-water depth), seawater $\varepsilon_{Nd}(t)$ signatures were close to those recorded at Site 249 during state 1 and range from −5.4 to −3.8. These $\varepsilon_{Nd}(t)$ signatures were markedly more radiogenic than contemporaneous detrital $\varepsilon_{Nd}(t)$ values of −9.0 and −9.2.

By ∼118 Ma the deposition of gray shale with TOC contents ≤3% commenced at Sites 361, 511, and Hole 327A. This marks the onset of phase 2, during which seawater $\varepsilon_{Nd}(t)$ signatures of -3 ± 0.5 were recorded at Sites 361 and 511, corresponding to a shift to more radiogenic values compared to phase 1. Seawater $\varepsilon_{Nd}(t)$ values at Hole 327A were slightly less radiogenic than at Site 511, ranging between −4.2 and −3.8. At Hole 693A, seawater $\varepsilon_{Nd}(t)$ signatures shifted from −4.2 to ∼−3 during phase 2 and thus converged with the $\varepsilon_{Nd}(t)$ signatures at Sites 511 and 361. Detrital material with $\varepsilon_{Nd}(t)$ values of −6.7, −6.8, and −6.3 was deposited at Sites 361, 511, and Hole 693A, respectively. Concurrent with the shift in seawater $\varepsilon_{Nd}(t)$ signatures recorded at Hole 693A, gray shale sedimentation with TOC contents averaging to 1.8% ceased and was replaced by diatomites containing <1% TOC.

By ∼110 Ma, at the base of phase 3 (∼110 Ma to ∼100.5 Ma), seawater $\varepsilon_{Nd}(t)$ values at Sites 511, 361, and Hole 327A, had decreased by 2.5 units, after which they remained constant near values of −4.5. Contemporaneous detrital $\varepsilon_{Nd}(t)$ values show an

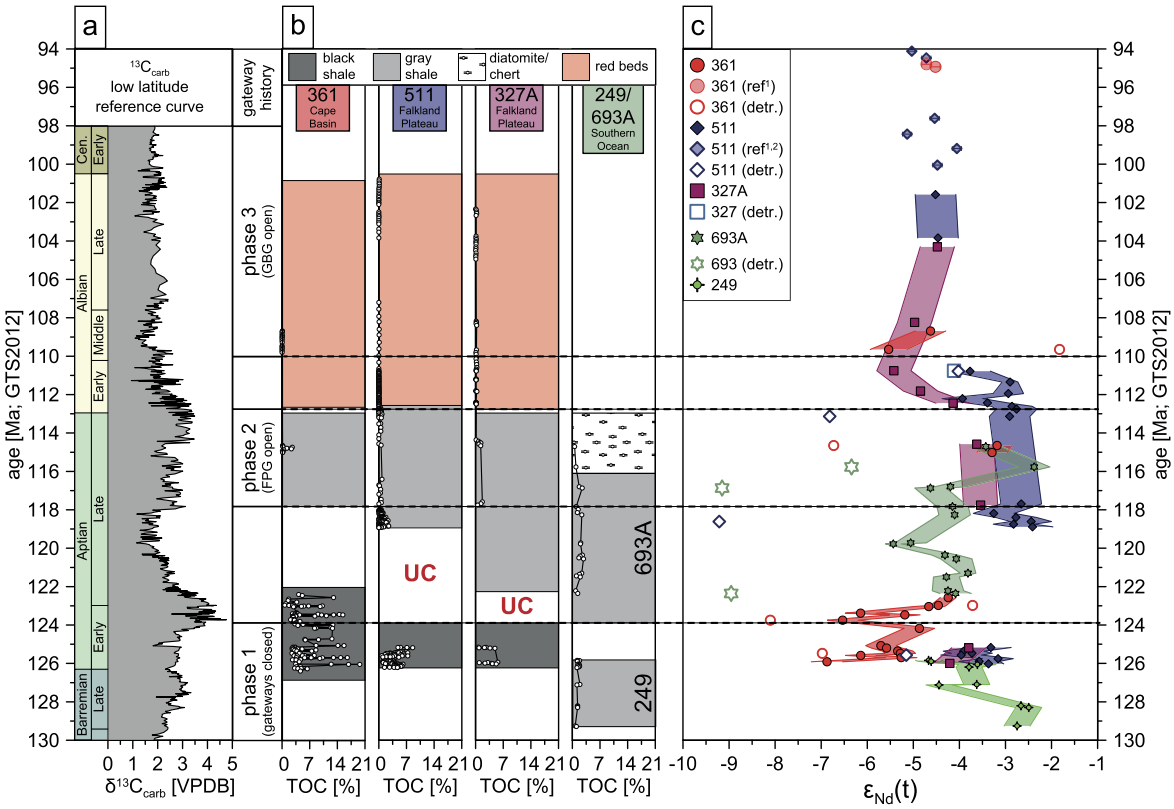

Fig. 3. (a) Low latitude carbon isotope record curve compiled by Herrle et al. (2015), (b) total organic carbon contents at DSDP Site 361, DSDP Site 511, DSDP Hole 327A, ODP Hole 693A, and DSDP Site 249 plotted against age. Background shading represents dominant lithology. The height of the lithological columns reflects potential age range of each stratigraphic segment (Fig. 2) (c) Evolution of seawater Nd isotope signatures (filled symbols) and detrital Nd isotope signatures (open symbols) at all study sites. Shaded areas represent 2SD error ranges of seawater Nd isotope signatures. Late Albian to Cenomanian seawater Nd isotope signatures of DSDP Site 361 and DSDP Site 511 were taken from the literature (ref[1]: Murphy and Thomas (2013), ref[2]: Robinson et al. (2010)). Age constraints for literature data were updated to GTS2012 by Moiroud et al. (2016).

opposite trend to more radiogenic values. This shift in seawater $\varepsilon_{Nd}(t)$ was accompanied by the onset of red bed deposition on the Falkland Plateau and in the Cape Basin during the Early Albian, which continued into the Late Albian.

3.2. Simulated circulation

The circulation patterns simulated by the KCM for the Late Aptian to Early Albian are shown in Fig. 4 and indicate that upper ocean waters in the Southern Ocean were dominated by a zonal current advecting cold and fresh waters from the high-latitude South Pacific via the narrow Antarctic Peninsula-Patagonia passage (hereafter called proto-Drake Passage). The total volume transport via this gateway amounted to ~20 Sv (1 Sv ≅ 10^6 m^3/s) and was restricted to the upper 1400 m. A surface current of 3.5 Sv turned northward entering the South Atlantic basin. Evaporation rates exceeded local precipitation north of 45°S, thereby increasing surface densities along the shelf in the central and northern parts of the Cape-Argentine Basin. These warm, saline surface waters were subducted to intermediate depths and formed a subsurface temperature and salinity maximum between 400–800 m water depth. The newly formed South Atlantic intermediate water flowed southwards and exited into the Southern Ocean via the Falkland Plateau Basin, at depths >100 m. Below this shallow meridional overturning circulation cell with an overall strength of ~1.5 Sv, bottom waters in the South Atlantic, Weddell Sea and Mozambique Basin were isolated and characterized by overall sluggish circulation.

4. Discussion

The magnitude of OC burial is controlled by a complex interplay of productivity, preservation, and dilution, all of which are strongly influenced by local oceanography and hydrology. Considering that our records were obtained from diverse depositional settings, inter-site TOC contrasts may therefore reflect differences in these local paleoenvironmental conditions. Hence, we focus on relative changes in TOC content at each site and use a broad classification to describe lithological changes (i.e., black shale >3% TOC, gray shale 0.5–3% TOC, red bed <0.5% TOC). Local oceanography and hydrology varied considerably on sub-tectonic time scales (<10^6 to 10^7 yr), often expressed as centimeter to meter-scale heterogeneities in TOC content (Wagner et al., 2013). Similar variations in TOC content and fluctuations between organic matter from different sources (e.g. marine, terrestrial, microbial), exist at some of our study sites, indicating additional driving mechanism acting on ten to hundred thousand year time scales, the discussion of which is, however, beyond the scope of our study.

Our records reveal a logical succession of persistent TOC decreases on multi-million year time scales, indicating a tectonic control on large-scale organic burial. These successive decreases in TOC occurred concomitantly with shifts in seawater $\varepsilon_{Nd}(t)$, supporting a close link between OC burial and bottom water mass provenance and/or mixing. Hence, we propose that deep water circulation played a critical role in preconditioning these emerging ocean basins for enhanced OC preservation via changes in deep water ventilation, consistent with previous studies (Behrooz et al., 2018; Donnadieu et al., 2016). Based on comparison with paleo-bathymetric reconstructions (Pérez-Díaz and Eagles, 2017),

we identify changes in continent-ocean configuration as the main drivers of deep water circulation. We develop conceptual models of ocean circulation for three stratigraphic phases representing major stages of gateway evolution and illustrate how these changes in circulation patterns affected large-scale OC burial.

4.1. Phase 1: isolated basins during the Late Barremian and Early Aptian

Late Barremian to Early Aptian paleo-bathymetric reconstructions suggest that water mass exchange between the South Atlantic and Southern Ocean basins was restricted, with shallow water connections across the Falkland Plateau (Pérez-Díaz and Eagles, 2017). Hence, Site 511 and Hole 327A on the Falkland Plateau represent strategic locations during phase 1 (∼129 Ma to ∼124 Ma). The seawater $\varepsilon_{Nd}(t)$ signatures at both sites were indistinguishable from those at Site 249, but different from those recorded at Cape Basin Site 361. Considering the similar water depths of Sites 249, 511 and Hole 327A, the data suggest a common intermediate water mass both on the Falkland Plateau and the Mozambique Ridge. Contrasting radiogenic seawater $\varepsilon_{Nd}(t)$ signatures and less radiogenic detrital $\varepsilon_{Nd}(t)$ signatures at Site 511 indicate that intermediate water masses did not obtain their Nd isotope composition from local weathering inputs, but rather originated further afield. Today, deep water masses with similarly radiogenic Nd isotope composition (ε_{Nd} of ∼−4 to −7) enter the Atlantic sector of the Southern Ocean across the Drake Passage as part of the Antarctic Circumpolar Current (ACC). ACC deep waters originate from the confluence of North Pacific Deep Water (NPDW; Molina-Kescher et al. (2014)), South Pacific Deep Water (SPDW; Albarède and Goldstein (1992)), and Ross Sea Deep Water (RSDP; Basak et al. (2015)) in the South Pacific. SPDW and RSDW originate from locations along the Antarctic coast, where they are imprinted with a relatively radiogenic Nd isotope composition, derived from the erosional input of radiogenic Nd from volcanic and intrusive rocks of the Antarctic Peninsula (ε_{Nd} of −5.5 to +0.9; Jeandel et al. (2007); Roy et al. (2007)). NPDW receives its radiogenic Nd isotope compositions from exchange with volcanic rocks prevailing around the North Pacific. During the Early Cretaceous, surface waters along the South Pacific Antarctic coast likely received similar erosional input of radiogenic Nd, given that $^{40}Ar/^{39}Ar$ dating of hornblende grains in modern surface sediments yield ages of ∼200 Ma (Roy et al., 2007). This suggests that the volcanic rocks along the Antarctic Peninsula and the Pacific Antarctic coast were already present in the Early Cretaceous, consistent with $\varepsilon_{Nd}(t)$ signatures of Late Cretaceous South Pacific water masses (MacLeod et al., 2008; Moiroud et al., 2016; Thomas et al., 2014) and sparse Early Cretaceous Pacific data (Murphy and Thomas, 2012; Robinson et al., 2010) that show $\varepsilon_{Nd}(t)$ values near −4. Although the Early Cretaceous position of the Antarctic Peninsula and the depth and width of the proto-Drake Passage are poorly constrained (Miller, 2007), most reconstructions suggest that narrow and shallow connections existed during the Barremian to Albian (Eagles, 2016; Sewall et al., 2007). One potential pathway for water mass exchange between the Pacific and the Southern Ocean may have been the Rocas Verdes Basin (Fig. 1), which is known from outcrops in the Patagonian Andes (e.g., Dalziel et al., 1974). This basin was a SE-NW trending back-arc basin underlain by oceanic crust that opened along the Patagonian subduction zone during the Late Jurassic and Early Cretaceous with an estimated width of 100–300 km (Eagles, 2016; Winn, 1978). West to east transport of intermediate water masses through this proto-Drake Passage is supported by our modeling results (Fig. 4) and previous general circulation models (Donnadieu et al., 2016; Uenzelmann-Neben et al., 2016). Simulated volume transport of 20 Sv was, however, significantly lower than at present (∼140 Sv for Drake Passage; Koenig et al. (2016)) due to the reduced horizontal and in particular vertical extent of the early gateway. Given the similarity of the $\varepsilon_{Nd}(t)$ signatures expected for South Pacific intermediate water and those recorded on the Falkland Plateau and the Mozambique Ridge, we propose a Southern Pacific source of intermediate waters during phase 1, transported eastwards along the Falkland Plateau and the Mozambique Ridge (Fig. 6a).

Barremian sea water $\varepsilon_{Nd}(t)$ signatures of −3 to −2.5 at Site 249 partly deviated from the Pacific $\varepsilon_{Nd}(t)$ endmember of −4. To date, it is unclear whether this deviation reflects a local change in seawater $\varepsilon_{Nd}(t)$ on Mozambique Ridge or a different oceanographic situation in the entire Southern Ocean. In support of the first, recent studies indicate that the southern Mozambique Ridge (Fischer et al., 2016), composed of tholeiitic basalts with $\varepsilon_{Nd}(t)$ signatures >0 (Jacques et al., 2019), was emplaced during the Barremian. Pulses of increased volcanic activity can temporarily shift seawater $\varepsilon_{Nd}(t)$ signatures by up to several ε units as observed in similar settings such as on the Late Cretaceous Walvis Ridge (Voigt et al., 2013). Hence, we hypothesize that more radiogenic water mass $\varepsilon_{Nd}(t)$ signatures at Site 249 during the Barremian reflect interaction of local seawater with fresh basaltic material erupted during the emplacement of the southern Mozambique Ridge.

Site 361, located in the deep Cape Basin, recorded distinctly more negative seawater $\varepsilon_{Nd}(t)$ signatures than the Falkland Plateau during phase 1, supporting a different provenance and/or formation process of water masses in the deep South Atlantic. Our model indicates that stagnant conditions prevailed in the deep South Atlantic basin below a depth of 1400 m, where saline bottom waters accumulated. This is consistent with earlier studies (Arthur and Natland, 1979; Natland, 1978) that proposed highly saline bottom water based on authigenic clay mineral assemblages at Site 361. How and where these stagnant deep waters acquired their more negative Nd isotope composition remains difficult to assess. Arthur and Natland (1979) speculated that saline deep waters in the Cape-Argentine Basin formed by episodic spillover of brines from the Angola Basin to the north across the Walvis Ridge. The presence of highly saline waters in the Angola Basin at that time is supported by carbon isotope stratigraphy suggesting an Early Aptian age for salt deposition in the Campos and Santos Basin directly north of the Walvis Ridge (Tedeschi et al., 2017). However, if these brines were transported into the deep Cape-Argentine Basin remains unclear as the Early Aptian geometry of the Walvis Ridge is poorly constrained. Alternatively, bottom water $\varepsilon_{Nd}(t)$ in the Cape Basin may have been controlled by vertical cycling rather than lateral advection of Nd. Reversed scavenging, a process by which Nd is scavenged from surface waters by adsorption onto biogenic or lithogenic particles and released at depth, has been shown to affect bottom water $\varepsilon_{Nd}(t)$ in the modern ocean. Model results indicate that this process is of particular importance in the relatively sluggish North Pacific, while it is less important in the Atlantic Basin, where circulation is more vigorous (Arsouze et al., 2009; Siddall et al., 2008). Given that deep water circulation in the Aptian Cape Basin was probably sluggish to nearly stagnant, conditions may have been particularly conducive to reversed scavenging of Nd. In the modern central Angola Basin, vertical cycling of Nd with a negative ε_{Nd} signature is facilitated by organic matter supplied by the Congo River, which is remineralized upon deposition and Nd is released, thereby affecting the Nd isotope composition of ambient bottom waters (Rickli et al., 2009). At Site 361, Aptian palynomorph assemblages indicate high river run-off from the proximal African continent (Davey, 1978) and Rock-Eval data suggest a high abundance of terrigenous organic matter (Hartwig et al., 2012). These data indicate conditions similar to the modern Angola Basin, based on which we propose that Nd with an unradiogenic $\varepsilon_{Nd}(t)$ signature originating from weathering sources on the proximal southern African continent was supplied to the Early Cretaceous Cape Basin by westward draining rivers (e.g., Kounov et

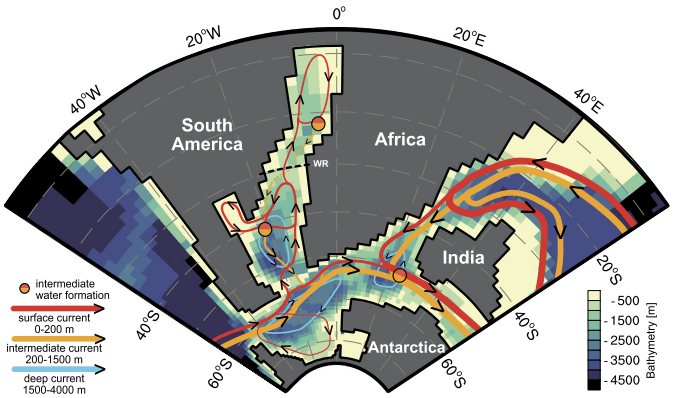

Fig. 4. Scheme of ocean circulation in the Early Cretaceous South Atlantic and Southern Ocean generated by the Kiel Climate Model. Boundary conditions represent a Late Aptian to Early Albian time slice with a closed Georgia Basin Gateway. Line width qualitatively represents the depth-integrated volume transport for the respective surface, intermediate and deep currents. The location of the Walvis Ridge in respect to the model geography is indicated by the dashed black line.

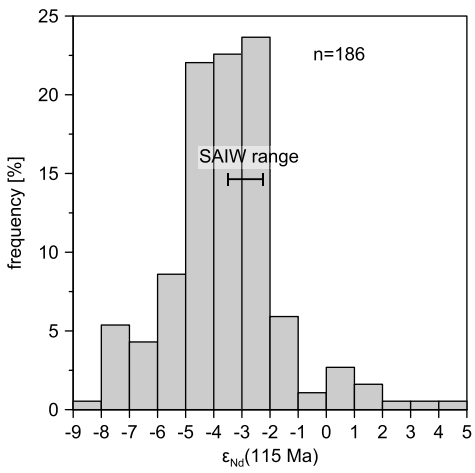

Fig. 5. Histogram showing the relative frequency of ε_{Nd} (calculated at 115 Ma) for Paraná basalts as reported in the literature ($n = 186$; Garland et al., 1996; Hawkesworth et al., 1988; Hawkesworth et al., 1986; Peate and Hawkesworth, 1996; Peate et al., 1999; Petrini et al., 1987; Piccirillo et al., 1990, 1989; Rämö et al., 2016; Rocha-Júnior et al., 2013; Turner et al., 1999). The horizontal bar indicates the ε_{Nd} signature inferred for South Atlantic Intermediate Water (SAIW).

al., 2008) and that reversed scavenging linked to terrigenous organic matter supplied Nd to the deep waters, thereby controlling local bottom water $\varepsilon_{Nd}(t)$. Seawater $\varepsilon_{Nd}(t)$ signatures recorded at Site 361 are overall consistent with the broad range of ε_{Nd} signatures reported for Paleozoic to Early Mesozoic sedimentary and volcanic rocks covering southern Africa (Dia et al., 1990).

The results imply that intermediate water mass exchange across the Falkland Plateau Basin was negligible during the Late Barremian and Early Aptian (Fig. 6a). The resulting hydrographic isolation of the South Atlantic basin likely resulted in a sluggish deep water circulation, which probably favored oxygen-deficient conditions, thus supporting the deposition of black shales with TOC contents >3% at Site 361. The Falkland Plateau Basin at that time had a semi-enclosed geometry, confined by the African continent and basement highs below the Falkland Islands and the Maurice Ewing Bank to the north, west, and east, respectively (Pérez-Díaz and Eagles, 2017). This geometry may have promoted a sluggish circulation within the central part of the basin, fostering the deposition of black shales with TOC contents of up to 8.6% at Site 511. In contrast, TOC contents on the Mozambique Ridge further east were significantly lower, consistent with a more exposed setting

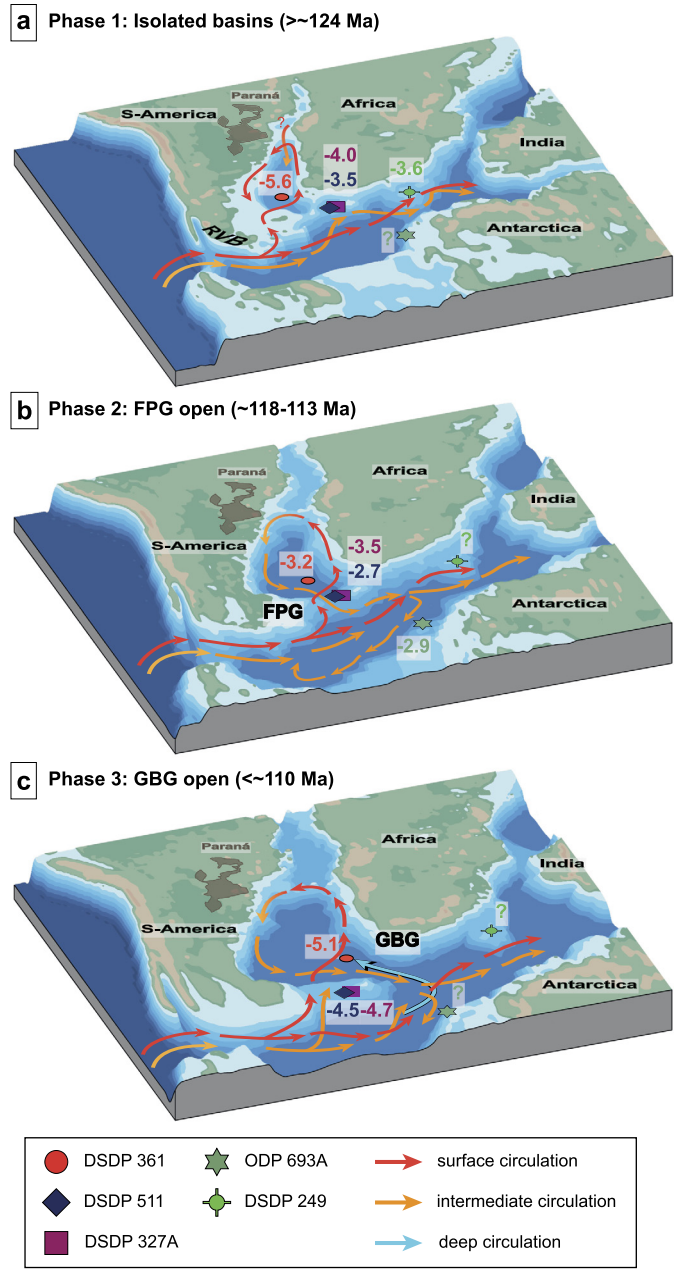

Fig. 6. Scheme of the proposed evolution of the circulation system in the Barremian to Albian South Atlantic and Southern Ocean (Please note that the topography shown is idealized and does not claim to be a detailed paleotopographic reconstruction): (a) phase 1 – circulation during the Late Barremian and Early Aptian prior to gateway opening (>~124 Ma), (b) phase 2 – circulation after the Falkland Plateau Gateway opened (between 118 Ma and 113 Ma), (c) phase 3 – circulation after the Georgia Basin Gateway opened (<~110 Ma). Numbers next to coring sites represent average seawater $\varepsilon_{Nd}(t)$ during each phase. RVB: Rocas Verdes Basin, FPG: Falkland Plateau Gateway, GBG: Georgia Basin Gateway.

below the core of the eastward flowing Southern Ocean intermediate water.

4.2. Phase 2: opening of the Falkland plateau gateway during the Late Aptian

By ~118 Ma, seawater $\varepsilon_{Nd}(t)$ signatures at Site 511 had shifted by ~1.5 ε_{Nd} units to more radiogenic signatures than during phase 1. The divergence of seawater $\varepsilon_{Nd}(t)$ at Site 511 from Southern Ocean signatures ($\varepsilon_{Nd}(t)$ of ~−4) suggests a change in water mass provenance with a reduced inflow of Pacific-sourced inter-

mediate water into the Falkland Plateau Basin to be replaced by an increasing admixture of northerly-sourced South Atlantic intermediate water. According to our model, South Atlantic intermediate water preferentially originated from locations along the South American shelf in the northern regions of the Cape-Argentine Basin. Surface waters in these regions would have predominantly received erosional input of radiogenic Nd from the Paraná large igneous province in the east, characterized by $\varepsilon_{Nd}(t)$ signatures of ~-5 to ~-2 (Fig. 5). Excess evaporation under subtropical climates would have increased the salinity of these surface waters originating from the Cape-Argentine margin, which then sank to form southward flowing South Atlantic intermediate water (Fig. 4). In accordance with paleo-bathymetric reconstructions suggesting that the Falkland Plateau Basin may have provided a pathway ($\leq$1000 m) for intermediate water mass exchange between the South Atlantic and Southern Ocean by the Late Aptian (Pérez-Díaz and Eagles, 2017), we attribute the shift in water mass provenance recorded at Site 511 to the opening of the Falkland Plateau Gateway, which thus must have been sufficiently wide and deep by at least $\sim$118 Ma (Fig. 6b). This is supported by our model, indicating export of South Atlantic intermediate water across the Falkland Plateau Basin into the Southern Ocean (Fig. 4).

At Site 361, $\varepsilon_{Nd}(t)$ signatures were close to those recorded at Site 511 and Hole 327A. Our preferred explanation for this convergence of $\varepsilon_{Nd}(t)$ signatures is enhanced admixture of South Atlantic intermediate waters to the deeper water column, which may have been caused by intensified overturning in the South Atlantic in response to the Falkland Plateau Gateway opening.

Between $\sim$124 Ma to $\sim$118 Ma, seawater $\varepsilon_{Nd}(t)$ signatures at Hole 693A were similar to those recorded at Site 249 during phase 1, showing that a common intermediate water body with an $\varepsilon_{Nd}(t)$ signature of ~-4 existed in the Southern Ocean prior to $\sim$118 Ma. During phase 2 ($\sim$118 Ma to $\sim$113 Ma), seawater $\varepsilon_{Nd}(t)$ signatures at Hole 693A shifted to ~-2.9, consistent with intensified admixture of South Atlantic intermediate water ($\varepsilon_{Nd}(t)$ of ~-2.5) to Pacific-sourced intermediate water ($\varepsilon_{Nd}(t)$ of ~-4). This efficient mixing of South Atlantic and Southern Ocean intermediate water masses implies that the opening of the Falkland Plateau Gateway had a profound impact on the composition of the intermediate water body in the Southern Ocean.

Black shale deposition at Site 511 ceased with the onset of South Atlantic intermediate water mass throughflow across the Falkland Plateau Gateway (Fig. 3). The close correspondence of the shift in water mass provenance and cessation of black shale deposition suggests the onset of bottom water ventilation causing a marked change in redox conditions in the Falkland Plateau Basin. Enhanced vertical mixing of water masses in the Cape Basin as indicated by radiogenic $\varepsilon_{Nd}(t)$ signatures at Site 361, was likely accompanied by increased ventilation of the deeper basin, thereby inducing a shift from black shale to gray shale deposition. Enhanced admixture of South Atlantic intermediate waters to the Southern Ocean, evidenced by radiogenic $\varepsilon_{Nd}(t)$ signatures at Hole 693A, may have altered the water column structure in the Weddell Sea. Warm and saline South Atlantic surface and intermediate waters entering the Weddell Sea may have diminished the density gradient between surface and deep waters, causing weakening of stratification along Antarctica. Enhanced vertical mixing would have delivered oxygen to the Antarctic slope and shelf, thus terminating gray shale deposition at Hole 693A. Although this sequence of changes requires further validation, it is supported by the occurrence of the unusually rich diatom flora observed in low TOC sediments of Hole 693A (Gersonde and Harwood, 1990). While diatoms are largely absent from the underlying gray shales, their sudden appearance in the low TOC sediments may be consistent with enhanced turbidity and intensified admixture of nutrients from the subsurface water column to the photic zone caused by vertical convection.

4.3. Phase 3: opening of the Georgia basin gateway in the Early Albian

Between $\sim$113 Ma and $\sim$110 Ma, seawater $\varepsilon_{Nd}(t)$ at Sites 361, 511, and Hole 327A consistently decreased to values around -4.5 and then remained constant throughout phase 3 ($\sim$110 Ma to 100.5 Ma) and until the Turonian (Murphy and Thomas, 2013; Robinson et al., 2010). This long term trend indicates a transition in deep and intermediate water circulation, followed by a persistent stability. Consistent with paleo-bathymetric reconstructions (Pérez-Díaz and Eagles, 2017), we propose that the Georgia Basin Gateway opening, linked to the detachment of the Maurice Ewing Bank from the African continent, was completed by $\sim$110 Ma and was the final step permitting unrestricted deep water mass exchange between the Southern Ocean and South Atlantic. Southern Pacific $\varepsilon_{Nd}(t)$ signatures of ~-4 recorded at the Falkland Plateau (Hole 327A and Site 511) suggest a reversal from southward to northward intermediate water flow across the Falkland Plateau Gateway, which possibly indicates that the outflow of South Atlantic intermediate water was redirected to the Georgia Basin Gateway. This is supported by modeling experiments indicating that a northward flow of upper Pacific waters across the Falkland Plateau into the South Atlantic was established by at least Late Cenomanian times (Uenzelmann-Neben et al., 2016). Modeling further indicates that a net northward deep water flow ($\geq$1000 m) across the Georgia Basin Gateway was initiated by the Late Cenomanian (Donnadieu et al., 2016; Uenzelmann-Neben et al., 2016), which is a plausible explanation for Southern Ocean $\varepsilon_{Nd}(t)$ signatures of ~-4 recorded at Site 361.

The onset of red bed deposition at Sites 361, 511, and Hole 327A during phase 3 documents that the opening of the Georgia Basin Gateway induced a major redox change in both the Cape and the Falkland Plateau Basins that resulted in a large-scale decrease of OC burial.

4.4. Implications for the carbon cycle and climate

Studies based on TEX_{86} paleothermometry (McAnena et al., 2013), stable oxygen isotopes (Clarke and Jenkyns, 1999; Huber et al., 2011), and plankton distribution (Bottini et al., 2015) indicate a transition from a globally cool climate during the Late Aptian to warmer temperatures during the Early Albian. Supported by biogeochemical modeling, McAnena et al. (2013) proposed that this warming was at least partly attributable to reduced marine OC burial in the South Atlantic and Southern Ocean. Our data do not allow us to directly quantify the consequences of local OC burial on the global carbon cycle and climate. However, they indicate a decline of large-scale OC burial in the South Atlantic across the Aptian/Albian boundary, concomitant with global warming. This synchronicity may well point to a causal relationship, which, however, requires corroboration by advanced biogeochemical modeling. This study provides a robust proxy database to constrain future biogeochemical modeling studies and a temporal framework for linking these models to trends in the global carbon-climate cycle.

5. Conclusions

Our study provides a comprehensive reconstruction of the ocean circulation patterns in the Barremian to Albian South Atlantic and Southern Oceans, derived from newly obtained seawater Nd isotope data and supported by general circulation modeling. We identify the evolution of marine gateways as the main driver of ocean circulation changes in the emerging South Atlantic and Southern Ocean and constrain the timing (within the

limits of stratigraphic uncertainty) of the opening of two key marine gateways connecting the Cretaceous high and low latitude ocean. The Falkland Plateau Gateway opened in the early Late Aptian (between ∼118 and ∼113 Ma) and provided a pathway for intermediate water mass exchange between the low latitude Cape-Argentine Basin and high latitude Southern Ocean. In the Early Albian (∼110 Ma), the Georgia Basin Gateway opened when the eastern edge of the Falkland Plateau (i.e., Maurice Ewing Bank) detached from the African continent, thereby enabling unrestricted deep water circulation. The temporal evolution of $\varepsilon_{Nd}(t)$ in the South Atlantic and Southern Ocean is best explained by a continuous water mass exchange between the Pacific and Southern Ocean during the investigated time interval, indicating the existence of a shallow proto-Drake Passage between South America and the Antarctic Peninsula. The opening of the Georgia Basin Gateways caused a large-scale reduction of OC burial in the South Atlantic that coincided with a major global warming across the Aptian/Albian boundary. Based on this synchronicity, we suggest that OC burial in the emerging South Atlantic has contributed significantly to trends in the global carbon cycle and climate. This hypothesis can be tested by future biogeochemical modeling, for which our study provides the conceptual and temporal framework.

Acknowledgements

We thank Nicole Mantke for TOC analyses. Model integrations were conducted at the Computing Center of Kiel University. We thank Janine Blöhdorn for generating most of the Cretaceous boundary conditions for the model and Stefan Hagemann for constructing the parameters for the hydrological discharge model. This research used samples provided by the Deep Sea Drilling Project and the Ocean Drilling Project. ODP has been sponsored by the U.S. National Science Foundation and participating countries under the management of Joint Oceanographic Institutions. This work was funded by the German Research Foundation (grant number HO2188/9) granted to PH, JOH and SF.

Appendix A. Supplementary material

Supplementary material related to this article can be found online at https://doi.org/10.1016/j.epsl.2019.115890.

References

Albarède, F., Goldstein, S.L., 1992. World map of Nd isotopes in sea-floor ferromanganese deposits. Geology 20, 761–763.
Arsouze, T., Dutay, J., Lacan, F., Jeandel, C., 2009. Reconstructing the Nd oceanic cycle using a coupled dynamical-biogeochemical model. Biogeosciences 6, 2829–2846.
Arthur, M.A., Natland, J.H., 1979. Carbonaceous sediments in the North and South Atlantic: the role of salinity in stable stratification of Early Cretaceous basins. In: Talwani, M., Hay, W.W., Ryan, W.B.F. (Eds.), Deep Drilling Results in the Atlantic Ocean: Continental Margins and Paleoenvironment. American Geophysical Union, Washington, DC, pp. 375–401.
Barker, P.F., Dalziel, I.W.D., Dinkelman, M.G., Elliot, D.H., Gombos Jr., A.M., Lonardi, A., Plafker, G., Tarney, J., Thompson, R.W., Tjalsma, R.C., von der Borch, C.C., Wise Jr., S.W., Harris, W.K., Sliter, W.V., 1977. Site 327. In: Barker, P.F., Dalziel, I.W.D. (Eds.), Initial Reports of the Deep Sea Drilling Project, vol. 36. U.S. Government Printing Office, Washington, DC, pp. 27–86.
Barker, P.F., Kennett, J.P., O'Connell, S., Berkowitz, S., Bryant, W.R., Burckle, L.H., Egeberg, P.K., Fütterer, D.K., Gersonde, R.E., Golovchenko, X., Hamilton, N., Lawver, L., Lazarus, D.B., Lonsdale, M., Mohr, B.A., Nagao, T., Pereira, C.P.G., Pudsey, C.J., Robert, C.M., Schandl, E.S., Spiess, V., Stott, L.D., Thomas, E., Thompson, K.F.M., Wise Jr., S.W., 1988. Site 693. In: Barker, P.F., Kennett, J.P. (Eds.), Proceedings of the Ocean Drilling Program, Initial Reports, vol. 113. Ocean Drilling Program, College Station, pp. 329–447.
Barrat, J.A., Keller, F., Amossé, J., Taylor, R.N., Nesbitt, R.W., Hirata, T., 1996. Determination of rare earth elements in sixteen silicate reference samples by ICP-MS after Tm addition and ion exchange separation. Geostand. Newsl. 20, 133–139.
Basak, C., Pahnke, K., Frank, M., Lamy, F., Gersonde, R., 2015. Neodymium isotopic characterization of Ross Sea Bottom Water and its advection through the southern, South Pacific. Earth Planet. Sci. Lett. 419, 211–221.
Basov, I.A., Krasheninnikov, V.A., 1983. Benthic foraminifers in Mesozoic and Cenozoic sediments of the southwestern Atlantic as an indicator of paleoenvironment, Deep Sea Drilling Project Leg 71. In: Ludwig, W.J., Krasheninnikov, V.A. (Eds.), Initial Reports of the Deep Sea Drilling Project, vol. 71. U.S. Government Printing Office, Washington, DC, pp. 739–787.
Bayon, G., Barrat, J.A., Etoubleau, J., Benoit, M., Bollinger, C., Révillon, S., 2009. Determination of rare earth elements, Sc, Y, Zr, Ba, Hf and Th in geological samples by ICP-MS after Tm addition and alkaline fusion. Geostand. Geoanal. Res. 33, 51–62.
Behrooz, L., Naafs, B.D.A., Dickson, A.J., Love, G.D., Batenburg, S.J., Pancost, R.D., 2018. Astronomically driven variations in depositional environments in the South Atlantic during the Early Cretaceous. Paleoceanogr. Paleoclimatol. 33, 894–912.
Berner, R.A., 1990. Atmospheric carbon dioxide levels over Phanerozoic time. Science 249, 1382–1386.
Blakey, R.C., 2008. Gondwana paleogeography from assembly to breakup—a 500 m.y. odyssey. In: Fielding, C.R., Frank, T.D., Isbell, J.L. (Eds.), Resolving the Late Paleozoic Ice Age in Time and Space. The Geological Society of America, Boulder, pp. 1–28.
Blaser, P., Lippold, J., Gutjahr, M., Frank, N., Link, J.M., Frank, M., 2016. Extracting foraminiferal seawater Nd isotope signatures from bulk deep sea sediment by chemical leaching. Chem. Geol. 439, 189–204.
Blöhdorn, J., 2013. Klima und Ozeanzirkulation der Frühen Kreide im Kiel Climate Model. Mathematisch-Naturwissenschaftliche Fakultät, Christian-Albrechts-Universität zu Kiel, Kiel, p. 121.
Bolli, H.M., Ryan, W.B.F., Foresman, J.B., Hottman, W.E., Kagami, H., Longoria, J.F., McKnight, B.K., Melguen, M., Natland, J.H., Proto Decima, F., Siesser, W.G., 1978. Cape Basin continental rise; Sites 360 and 361. In: Bolli, H.M., Ryan, W.B.F. (Eds.), Initial Reports of the Deep Sea Drilling Project, vol. 40. U.S. Government Printing Office, Washington, DC, pp. 29–182.
Bottini, C., Erba, E., Tiraboschi, D., Jenkyns, H.C., Schouten, S., Sinninghe Damsté, J.S., 2015. Climate variability and ocean fertility during the Aptian Stage. Clim. Past 11, 383–402.
Bown, P., Rutledge, D., Crux, J., Gallagher, L., 1998. Lower Cretaceous. In: Bown, P. (Ed.), Calcareous Nannofossil Biostratigraphy. Chapman & Hall/Kluwer Academic Publishers Group, London, pp. 86–131.
Clarke, L.J., Jenkyns, H.C., 1999. New oxygen isotope evidence for long-term Cretaceous climatic change in the Southern Hemisphere. Geology 27, 699–702.
Dalziel, I.W.D., de Wit, M.J., Palmer, K.F., 1974. Fossil marginal basin in the southern Andes. Nature 250, 291–294.
Davey, R.J., 1978. Marine Cretaceous palynology of Site 361, DSDP Leg 40, off southwestern Africa. In: Bolli, H.M., Ryan, W.B.F. (Eds.), Initial Reports of the Deep Sea Drilling Project, vol. 40. U.S. Government Printing Office, Washington, DC, pp. 883–913.
Dia, A., Allegre, C.J., Erlank, A.J., 1990. The development of continental crust through geological time: the South African case. Earth Planet. Sci. Lett. 98, 74–89.
Donnadieu, Y., Pucéat, E., Moiroud, M., Guillocheau, F., Deconinck, J.-F., 2016. A better-ventilated ocean triggered by Late Cretaceous changes in continental configuration. Nat. Commun. 7, 10316.
Dunay, R.E., Braham, W., Cooper, M.K.E., Lester, M., Tremolada, F., 2018. Micropalaeontological dating of the basal Cretaceous section of DSDP Site 249, Leg 25, Mozambique Ridge: implications for the timing of the southern Atlantic-Indian Ocean connection. J. Micropaleontol. 37, 305–316.
Eagles, G., 2016. Plate kinematics of the Rocas Verdes Basin and Patagonian orocline. Gondwana Res. 37, 98–109.
Fischer, M.D., Uenzelmann-Neben, G., Jacques, G., Werner, R., 2016. The Mozambique Ridge: a document of massive multi-stage magmatism. Geophys. J. Int. 208, 449–467.
Frank, M., 2002. Radiogenic isotopes: tracers of past ocean circulation and erosional input. Rev. Geophys. 40, 1–38.
Garland, F., Turner, S., Hawkesworth, C., 1996. Shifts in the source of the Paraná basalts through time. Lithos 37, 223–243.
Gersonde, R.E., Harwood, D.M., 1990. Lower Cretaceous diatoms from ODP Leg 113 Site 693 (Weddell Sea), part 1: vegetative cells. In: Barker, P.F., Kennett, J.P. (Eds.), Proceedings of the Ocean Drilling Program, Initial Reports, vol. 113. Ocean Drilling Program, College Station, pp. 365–402.
Gradstein, F.M., Ogg, J.G., Schmitz, M., Ogg, G., 2012. The Geologic Time Scale 2012. Elsevier, Amsterdam.
Hagemann, S., Dümenil, L., 1997. A parametrization of the lateral waterflow for the global scale. Clim. Dyn. 14, 17–31.
Hartwig, A., di Primio, R., Anka, Z., Horsfield, B., 2012. Source rock characteristics and compositional kinetic models of Cretaceous organic rich black shales offshore southwestern Africa. Org. Geochem. 51, 17–34.
Hawkesworth, C., Mantovani, M., Peate, D., 1988. Lithosphere remobilization during Paraná CFB magmatism. J. Petrol. (Spec. Vol.), 205–223.
Hawkesworth, C., Mantovani, M., Taylor, P., Palacz, Z., 1986. Evidence from the Paraná of south Brazil for a continental contribution to Dupal basalts. Nature 322, 356–359.
Herrle, J.O., Schröder-Adams, C.J., Davis, W., Pugh, A.T., Galloway, J.M., Fath, J., 2015. Mid-Cretaceous High Arctic stratigraphy, climate, and oceanic anoxic events. Geology 43, 403–406.

Holbourn, A., Kuhnt, W., Soeding, E., 2001. Atlantic paleobathymetry, paleoproductivity and paleocirculation in the late Albian: the benthic foraminiferal record. Palaeogeogr. Palaeoclimatol. Palaeoecol. 170, 171–196.
Huber, B.T., MacLeod, K.G., Gröcke, D.R., Kucera, M., 2011. Paleotemperature and paleosalinity inferences and chemostratigraphy across the Aptian/Albian boundary in the subtropical North Atlantic. Paleoceanogr. Paleoclimatol. 26.
Jacques, G., Hauff, F., Hoernle, K., Werner, R., Uenzelmann-Neben, G., Garbe-Schönberg, D., Fischer, M., 2019. Nature and origin of the Mozambique Ridge, SW Indian Ocean. Chem. Geol. 507, 9–22.
Jeandel, C., Arsouze, T., Lacan, F., Techine, P., Dutay, J.C., 2007. Isotopic Nd compositions and concentrations of the lithogenic inputs into the ocean: a compilation, with an emphasis on the margins. Chem. Geol. 239, 156–164.
Jing, D., Bainian, S., 2018. Early Cretaceous atmospheric CO_2 estimates based on stomatal index of Pseudofrenelopsis papillosa (Cheirolepidiaceae) from southeast China. Cretac. Res. 85, 232–242.
Katz, B.J., Mello, M.R., 2000. Petroleum Systems of South Atlantic Marginal Basins. The American Association of Petroleum Geologists and PETROBRAS, Tulsa.
Koenig, Z., Provost, C., Park, Y.H., Ferrari, R., Sennéchael, N., 2016. Anatomy of the Antarctic Circumpolar Current volume transports through Drake Passage. J. Geophys. Res., Oceans 121, 2572–2595.
Kounov, A., Viola, G., De Wit, M., Andreoli, M., 2008. A Mid Cretaceous paleo-Karoo River valley across the Knersvlakte plain (northwestern coast of South Africa): evidence from apatite fission-track analysis. S. Afr. J. Geol. 111, 409–420.
Le Fèvre, B., Pin, C., 2005. A straightforward separation scheme for concomitant Lu–Hf and Sm–Nd isotope ratio and isotope dilution analysis. Anal. Chim. Acta 543, 209–221.
Leckie, R.M., 1990. Middle Cretaceous planktonic foraminifers of the Antarctic margin; hole 693A, ODP Leg 113. In: Barker, P.F., Kennett, J.P. (Eds.), Proceedings of the Ocean Drilling Program, Initial Reports, vol. 113. Ocean Drilling Program, College Station, pp. 319–324.
Ling, H.F., Burton, K.W., O'Nions, R.K., Kamber, B.S., Von Blanckenburg, F., Gibb, A.J., Hein, J.R., 1997. Evolution of Nd and Pb isotopes in Central Pacific seawater from ferromanganese crusts. Earth Planet. Sci. Lett. 146, 1–12.
Ludwig, W.J., Krasheninnikov, V.A., Basov, I.A., Bayer, U., Bloemendal, J., Bornhold, B., Ciesielski, P.F., Goldstein, E.H., Robert, C., Salloway, J., Usher, J.L., von der Dick, H., Weaver, F.M., 1983. Site 511. In: Ludwig, W.J., Krasheninnikov, V.A. (Eds.), Initial Reports of the Deep Sea Drilling Project, vol. 71. U.S. Government Printing Office, Washington, DC, pp. 21–109.
MacLeod, K.G., Martin, E.E., Blair, S.W., 2008. Nd isotopic excursion across Cretaceous ocean anoxic event 2 (Cenomanian-Turonian) in the tropical North Atlantic. Geology 36, 811–814.
Madec, G.V., 2008. NEMO ocean engine. Note du Pôle de modélisation. Institut Pierre-Simon Laplace (IPSL), France, Paris.
Matthews, K.J., Maloney, K.T., Zahirovic, S., Williams, S.E., Seton, M., Mueller, R.D., 2016. Global plate boundary evolution and kinematics since the late Paleozoic. Glob. Planet. Change 146, 226–250.
McAnena, A., Flögel, S., Hofmann, P., Herrle, J.O., Griesand, A., Pross, J., Talbot, H.M., Rethemeyer, J., Wallmann, K., Wagner, T., 2013. Atlantic cooling associated with a marine biotic crisis during the mid-Cretaceous period. Nat. Geosci. 6, 558–561.
Melguen, M., 1978. Facies evolution, carbonate dissolution cycles in sediments from the eastern South Atlantic (DSDP Leg 40) since the Early Cretaceous. In: Bolli, H.M., Ryan, W.B.F. (Eds.), Initial Reports of the Deep Sea Drilling Project, vol. 40. U.S. Government Printing Office, Washington, DC, pp. 981–1024.
Miller, H., 2007. History of views on the relative positions of Antarctica and South America: a 100-year tango between Patagonia and the Antarctic Peninsula. In: Cooper, A.K., Raymond, C.R. (Eds.), Antarctica: A Keystone in a Changing World—Online Proceedings for the 10th International Symposium on Antarctic Earth Sciences, p. 4. USGS Open-File Report 2007-1047-SRP-041, Short Research Paper 041.
Moiroud, M., Pucéat, E., Donnadieu, Y., Bayon, G., Guiraud, M., Voigt, S., Deconinck, J.-F., Monna, F., 2016. Evolution of neodymium isotopic signature of seawater during the Late Cretaceous: implications for intermediate and deep circulation. Gondwana Res. 36, 503–522.
Molina-Kescher, M., Frank, M., Hathorne, E., 2014. South Pacific dissolved Nd isotope compositions and rare earth element distributions: water mass mixing versus biogeochemical cycling. Geochim. Cosmochim. Acta 127, 171–189.
Müller, R.D., Sdrolias, M., Gaina, C., Steinberger, B., Heine, C., 2008. Long-term sea-level fluctuations driven by ocean basin dynamics. Science 319, 1357–1362.
Murphy, D.P., Thomas, D.J., 2012. Cretaceous deep-water formation in the Indian sector of the Southern Ocean. Paleoceanography 27, PA1211.
Murphy, D.P., Thomas, D.J., 2013. The evolution of Late Cretaceous deep-ocean circulation in the Atlantic basins: neodymium isotope evidence from South Atlantic drill sites for tectonic controls. Geochem. Geophys. Geosyst. 14, 5323–5340.
Natland, J.H., 1978. Composition, provenance, and diagenesis of Cretaceous clastic sediments drilled on the Atlantic continental rise off Southern Africa, DSDP Site 361; implications for the early circulation of the South Atlantic. In: Bolli, H.M., Ryan, W.B.F. (Eds.), Initial Reports of the Deep Sea Drilling Project, vol. 40. U.S. Government Printing Office, Washington, DC, pp. 1025–1061.
Park, W., Keenlyside, N., Latif, M., Ströh, A., Redler, R., Roeckner, E., Madec, G., 2009. Tropical Pacific climate and its response to global warming in the Kiel Climate Model. J. Climate 22, 71–92.
Peate, D.W., Hawkesworth, C.J., 1996. Lithospheric to asthenospheric transition in low-Ti flood basalts from southern Paraná, Brazil. Chem. Geol. 127, 1–24.
Peate, D.W., Hawkesworth, C.J., Mantovani, M.M., Rogers, N.W., Turner, S.P., 1999. Petrogenesis and stratigraphy of the high-Ti/Y Urubici magma type in the Paraná flood basalt province and implications for the nature of 'Dupal'-type mantle in the South Atlantic region. J. Petrol. 40, 451–473.
Perch-Nielsen, K., 1985. Mesozoic calcareous nannofossils. In: Bolli, H., Saunders, J., Perch-Nielsen, K. (Eds.), Plankton Stratigraphy. Cambridge University Press, Cambridge, pp. 329–426.
Petrini, R., Civetta, L., Piccirillo, E., Bellieni, G., Comin-Chiaramonti, P., Marques, L.S., Melfi, A.J., 1987. Mantle heterogeneity and crustal contamination in the genesis of low-Ti continental flood basalts from the Paraná plateau (Brazil): Sr–Nd isotope and geochemical evidence. J. Petrol. 28, 701–726.
Pérez-Díaz, L., Eagles, G., 2017. South Atlantic paleobathymetry since early Cretaceous. Sci. Rep. 7, 11819.
Piccirillo, E., Bellieni, G., Cavazzini, G., Comin-Chiaramonti, P., Petrini, R., Melfi, A., Pinese, J., Zantadeschi, P., De Min, A., 1990. Lower Cretaceous tholeiitic dyke swarms from the Ponta Grossa Arch (southeast Brazil): petrology, Sr-Nd isotopes and genetic relationships with the Paraná flood volcanics. Chem. Geol. 89, 19–48.
Piccirillo, E., Civetta, L., Petrini, R., Longinelli, A., Bellieni, G., Comin-Chiaramonti, P., Marques, L.S., Melfi, A.J., 1989. Regional variations within the Paraná flood basalts (southern Brazil): evidence for subcontinental mantle heterogeneity and crustal contamination. Chem. Geol. 75, 103–122.
Piepgras, D.J., Wasserburg, G.J., 1980. Neodymium isotopic variations in seawater. Earth Planet. Sci. Lett. 50, 128–138.
Proto Decima, F., Medizza, F., Todesco, L., 1978. Southeastern Atlantic Leg 40 calcareous nannofossils. In: Bolli, H.M., Ryan, W.B.F. (Eds.), Initial Reports of the Deep Sea Drilling Project, vol. 40. U.S. Government Printing Office, Washington, DC, pp. 571–634.
Rämö, O.T., Heikkilä, P.A., Pulkkinen, A.H., 2016. Geochemistry of Paraná-Etendeka basalts from Misiones, Argentina: some new insights into the petrogenesis of high-Ti continental flood basalts. J. South Am. Earth Sci. 67, 25–39.
Rickli, J., Frank, M., Halliday, A.N., 2009. The hafnium–neodymium isotopic composition of Atlantic seawater. Earth Planet. Sci. Lett. 280, 118–127.
Robinson, S.A., Murphy, D.P., Vance, D., Thomas, D.J., 2010. Formation of "Southern Component Water" in the Late Cretaceous: evidence from Nd-isotopes. Geology 38, 871–874.
Rocha-Júnior, E.R.V., Marques, L.S., Babinski, M., Nardy, A.J.R., Figueiredo, A.M.G., Machado, F.B., 2013. Sr–Nd–Pb isotopic constraints on the nature of the mantle sources involved in the genesis of the high-Ti tholeiites from northern Paraná Continental Flood Basalts (Brazil). J. South Am. Earth Sci. 46, 9–25.
Roeckner, E., Bäuml, G., Bonaventura, L., Brokopf, R., Esch, M., Giorgetta, M., Hagemann, S., Kirchner, I., Kornblueh, L., Manzini, E., 2003. The Atmospheric General Circulation Model ECHAM 5, Part I: Model Description. Max Planck Institute for Meteorology Report, Max Planck Institute for Meteorology, Hamburg, p. 140.
Roy, M., van de Flierdt, T., Hemming, S.R., Goldstein, S.L., 2007. $^{40}Ar/^{39}Ar$ ages of hornblende grains and bulk Sm/Nd isotopes of circum-Antarctic glacio-marine sediments: implications for sediment provenance in the Southern Ocean. Chem. Geol. 244, 507–519.
Sewall, J.O., van de Wal, R.S.W., van der Zwan, K., van Oosterhout, C., Dijkstra, H.A., Scotese, C.R., 2007. Climate model boundary conditions for four Cretaceous time slices. Clim. Past 3, 647–657.
Siddall, M., Khatiwala, S., van de Flierdt, T., Jones, K., Goldstein, S.L., Hemming, S., Anderson, R.F., 2008. Towards explaining the Nd paradox using reversible scavenging in an ocean general circulation model. Earth Planet. Sci. Lett. 274, 448–461.
Tachikawa, K., Jeandel, C., Roy-Barman, M., 1999. A new approach to the Nd residence time in the ocean: the role of atmospheric inputs. Earth Planet. Sci. Lett. 170, 433–446.
Tanaka, T., Togashi, S., Kamioka, H., Amakawa, H., Kagami, H., Hamamoto, T., Yuhara, M., Orihashi, Y., Yoneda, S., Shimizu, H., 2000. JNdi-1: a neodymium isotopic reference in consistency with LaJolla neodymium. Chem. Geol. 168, 279–281.
Taylor, S.R., McLennan, S.M., 1985. The Continental Crust: Its Composition and Evolution. Blackwell Scientific Publications, Oxford.
Tedeschi, L.R., Jenkyns, H.C., Robinson, S.A., Sanjinés, A.E.S., Viviers, M.C., Quintaes, C.M.S.P., Vazquez, J.C., 2017. New age constraints on Aptian evaporites and carbonates from the South Atlantic: implications for Oceanic Anoxic Event 1a. Geology 45, 543–546.
Thomas, D.J., Korty, R., Huber, M., Schubert, J.A., Haines, B., 2014. Nd isotopic structure of the Pacific Ocean 70–30 Ma and numerical evidence for vigorous ocean circulation and ocean heat transport in a greenhouse world. Paleoceanography 29, 454–469.
Trabucho Alexandre, J., Hay, W.W., de Boer, P.L., 2012. Phanerozoic environments of black shale deposition and the Wilson Cycle. Solid Earth 3, 29–42.
Turner, S., Peate, D., Hawkesworth, C., Mantovani, M., 1999. Chemical stratigraphy of the Paraná basalt succession in western Uruguay: further evidence for the diachronous nature of the Paraná magma types. J. Geodyn. 28, 459–469.
Uenzelmann-Neben, G., Weber, T., Grützner, J., Thomas, M., 2016. Transition from the Cretaceous ocean to Cenozoic circulation in the western South Atlantic — a twofold reconstruction. Tectonophysics 716, 225–240.

Voigt, S., Jung, C., Friedrich, O., Frank, M., Teschner, C., Hoffmann, J., 2013. Tectonically restricted deep-ocean circulation at the end of the Cretaceous greenhouse. Earth Planet. Sci. Lett. 369, 169–177.

Wagner, T., Hofmann, P., Flögel, S., 2013. Marine black shale deposition and Hadley Cell dynamics: a conceptual framework for the Cretaceous Atlantic Ocean. Mar. Pet. Geol. 43, 222–238.

Wasserburg, G.J., Jacobsen, S.B., DePaolo, D.J., McCulloch, M.T., Wen, T., 1981. Precise determination of Sm/Nd ratios, Sm and Nd isotopic abundances in standard solutions. Geochim. Cosmochim. Acta 45, 2311–2323.

Weissert, H., 1981. The environment of deposition of black shales in the Early cretaceous an ongoing controversy. In: Warme, J.E., Douglas, R.G., Winterer, E.L. (Eds.), The Deep Sea Drilling Project: A Decade of Progress, pp. 547–560. SEPM Special Publication, Tulsa.

Winn, R.D., 1978. Upper Mesozoic flysch of Tierra del Fuego and South Georgia Island: a sedimentologic approach to lithosphere plate restoration. Geol. Soc. Am. Bull. 89, 533–547.

Wissler, L., Funk, H., Weissert, H., 2003. Response of Early Cretaceous carbonate platforms to changes in atmospheric carbon dioxide levels. Palaeogeogr. Palaeoclimatol. Palaeoecol. 200, 187–205.

Zimmerman, H.B., Boersma, A., McCoy, F.W., 1987. Carbonaceous sediments and palaeoenvironment of the Cretaceous South Atlantic Ocean. Geol. Soc. (Lond.) Spec. Publ. 26, 271–286.